ANALYSIS OF GAS TRANSPORT IN MOLECULARLY-MIXED COMPOSITE MEMBRANES

Matthew P. Rivera and Ryan P. Lively*

School of Chemical and Biomolecular Engineering, Georgia Institute of Technology, Atlanta, GA

Corresponding author: Ryan P. Lively; ryan.lively@chbe.gatech.edu

Permanent address: Ford Environment Science and Technology Building, 311 Ferst Dr NW, Atlanta, GA 30332

Abstract

Individual molecules with intrinsic porosity, such as porous organic cages (POCs), have significant potential to improve the performance of a variety of separations media. An exemplar application is the blending of POCs with polymers to make molecularly mixed composite membranes (MMCMs). The intimate interaction between individual cage molecules and polymer chains results in a "solid-solution" that avoids longstanding interfacial issues associated with mixed matrix membranes. Moreover, as the cages are soluble in polymer solutions, the processing of these composites can be easily adapted to established polymer-based technologies as concerns with two-phase processing systems are avoided. MMCMs are still a relatively new development, and underlying transport processes within the membrane are not well understood. Here, we offer a detailed interpretation of guest transport through these solid solutions. We demonstrate how the

presence of cage molecules affects polymer chain motions that can impact guest transport through the polymer phase. We also show how cage loading affects membrane free volume. We find that gas permeation deviates significantly from predictions made with the Maxwell model for mixed matrix membranes. POCs were found to significantly alter membrane properties in the polymer phase because of intimate molecular interactions between the POC and polymer, violating one of the Maxwell models underlying assumptions. This work provides preliminary information on the nature of guest transport in MMCMs to aid their future adaptation to industrially-relevant separation units.

Keywords

Molecularly-mixed composite membrane; Porous organic cage; Free volume; Polyimide; Gas separations

1. Introduction

One of the most active areas of separations science is the development of new microporous materials for challenging molecular separations. A recent development in this field is the creation of porous organic cages (POCs).[1] Exemplar microporous material classes include zeolites,[2] metal-organic frameworks,[3] or similar three-dimensional network structures. In these materials, the porosity is derived from the formation of extended network structures. In contrast, POCs form self-supported, intrinsic porosity that does not require any higher-order structure; in essence, they are permanently microporous molecules. Moreover, they are solution-processable. This characteristic can significantly streamline the deployment of these materials into existing manufacturing networks as they are unlikely to significantly disrupt existing solution processing techniques. Other classes

of organic molecules also have been noted to show intrinsic porosity.[4, 5] Notable examples include pillar[n]arenes,[6] calix[n]arenes,[5] and urea-macrocycles.[7] In these molecules, the opening into the guest-accessible cavity is often as wide as the cavity itself. Therefore, the adsorption of guest molecules is controlled solely by the geometry and chemistry of the cavity. On the other hand, cage molecules typically have windows that are smaller than the internal cavity and can be used to control guest diffusion. Also, the cage structure of POCs allows BET surface areas previously unobtainable (in some cases >2,000 m^2/g) in non-network molecular solids.[1, 8, 9] Thus, POCs and similar cage molecules allow much greater control over guest transport than other intrinsically porous molecules. POCs can be formed by several different mechanisms such as boronic acid condensation and alkyne metathesis but are most commonly formed via an imine condensation of amines and aldehydes with complementary geometry.[10, 11] Since their creation, several studies have demonstrated the ability of these materials to perform challenging separations.[12-14]

As noted earlier, POCs are solution-processable individual molecules, which provides many possibilities for the type of separation media and modality that these materials can be integrated into. A notable advance is the development of thin film composite (TFC) membranes from POCs by Cooper and co-workers.[15] Solutions of CC3, CC13, and CC3 derivatives were processed onto porous substrates via spincoating to create thin topcoats with only cage molecules. SEM images showed that the topcoats created uniform, apparently non-defective membranes. Separation performance for several gas pairs was tested and shown to have performance approaching Robeson's 2008 H_2/N_2 upper bound.

An application that we find to be especially intriguing is the potential for POCs to be used in polymer-based composite materials. Several examples of this have already been reported in the literature.[16-19] Most of these studies have focused on using POCs to make mixed matrix membranes (MMMs) in which POC *crystals* are dispersed throughout a polymer matrix. Niu and co-workers have created water purification membranes using the POC Noria to interfacially synthesize polyarylate and polyamide MMMs. They demonstrated that the presence of Noria in the membrane improved both water permeance and salt rejection over the membranes without Noria.[17, 19] Computational work by Doonan et al. further supports the ability of POC composite materials to improve performance over their pure polymer counterparts.[20] An exciting application in using POCs in composite membranes is the formation of molecularly-mixed composite membranes (MMCMs).[21, 22] MMCMs take full advantage of the solubility of POCs to make membranes that are "solid solutions" in which the POC *molecules* are homogeneously dispersed throughout the polymer matrix. MMCMs have the benefit of overcoming the compatibility issues seen in many composite materials[23] because the filler phase is intertwined with the polymer matrix at a molecular level.[24] For this application, POC derivatives, termed amorphous scrambled porous organic cage (ASPOCs), may be more appropriate. ASPOCs are made by using a mixture of diamine linkers in the cage synthesis to make different but isoreticular POCs. The steric hindrance from the different linkers prevents efficient packing of the cages into coordinated structures in the solid-state and leaves them as an amorphous powder.[25] The lack of long-range order benefits both solubility and BET surface area compared to crystalline POCs. MMCMs using ASPOCs and a commercial polyimide (Matrimid) have previously

demonstrated membrane homogeneity via Raman mapping, differential scanning calorimetry, and other techniques. The composites also had both higher permeance and rejection of polystyrene oligomers in a variety of solvents compared to native Matrimid.[16]

Since ASPOC-based MMCMs are a relatively new type of composite material, we believe that it is important to describe in detail our interpretation of molecular transport processes through these membranes. In this work, we attempt to shed light on this phenomenon by analyzing the results of gas permeation experiments through the lens of plasticization/antiplasticization effects. We have previously shown that at low concentrations, ASPOCs can act as antiplasticizers in glassy polymers; we believe this occurs via the POCs wedging themselves between polymer chains and subsequently inhibiting segmental motion.[16] nlike a traditional free-volume occupying antiplasticizer, the POC has a permanent void due to its internal cavity. Thus, the POC can potentially affect both chain mobility (by reducing it) and increase the fractional free volume of the resulting matrix. Hence, the approach to characterizing transport must be altered from traditional antiplasticization methods. We will also show that conventional models for estimating the permeability of composites, namely the Maxwell model, are not at all suitable for MMCMs.

2. Theory

2.1 The Sorption-Diffusion Model

To study transport through MMCMs, it is necessary to start with the well-known sorption-diffusion model.[26] Conceptually, the sorption-diffusion model states that for a species to permeate through a membrane, it must adsorb to the upstream side of the

membrane, diffuse through the length of the membrane, and then desorb from the downstream side, with the driving force provided by a chemical potential gradient across the membrane. Mathematically, it is given by Equation 1,

$$\mathbb{P} = \mathbb{S} * D \tag{1}$$

where $\mathbb{P}$ is permeability and is the product of $\mathbb{S}$, the solubility coefficient, and D, the diffusion coefficient. Solubility and diffusion coefficients can be determined by experiment. They can also be decomposed further to gain insight into the energetics of transport. Since permeation is an activated process, it follows an Arrhenius-type relationship with temperature, given in Equation 2.

$$\mathbb{P} = \mathbb{P}_0 \exp\left(-\frac{E_{\mathbb{P}}}{RT}\right) \tag{2}$$

In Equation 2, $\mathbb{P}_0$ is the permeation pre-exponential term and $E_{\mathbb{P}}$ is the activation energy of permeation. By measuring permeation over a range of temperatures, we can calculate the activation energy from plots of the natural log of the permeability vs. inverse temperature. This information provides a useful metric for understanding the underlying mechanisms of membrane transport for different penetrants.

Another important metric of membrane performance is selectivity. Selectivity is the ratio of the respective permeabilities of two components. By combining this ratio with Equation 1, Equation 3 is derived.

$$\alpha_{\frac{A}{B}} = \frac{\mathbb{P}_A}{\mathbb{P}_B} = \left(\frac{\mathbb{S}_A}{\mathbb{S}_B}\right) * \left(\frac{D_A}{D_B}\right) \tag{3}$$

Here, $\alpha_{\frac{A}{B}}$ is the permeation selectivity between component A and component B. From Equation 3, it is clear that the separation of two components is ultimately driven by differences in their sorption and diffusive behavior in the membrane. Hence, a thorough

understanding of sorption and diffusion behavior is necessary to understand membrane transport fully.

2.2 Molecular Fillers Influence on Membrane Free Volume

We hypothesize that the incorporation of molecular cage fillers into polymeric membranes affects transport by two primary mechanisms commonly discussed in the antiplasticization literature. Whereas plasticization indicates that a component present in a membrane has increased chain mobility, elasticity, and permeability, antiplasticization occurs when a diluent causes a reduction in chain mobility and permeability, thus effectively "hardening" the polymer.[27, 28] The first antiplasticization effect of interest is on the fractional free volume of the membrane. The generally accepted definition for the fractional free volume is given by Equation 4.[29-31]

$$V_{FFV} = \frac{\hat{V} - \hat{V}_0}{\hat{V}} \tag{4}$$

Here, V_{FFV} is the fractional free volume of the native polymer, $\hat{V}$ is the experimentally measured specific volume, and $\hat{V}_0$ is the specific volume of the material at 0 K, in other words, its theoretical minimum specific volume. $\hat{V}_0$ is determined from group contribution methods. The most commonly used method is proposed by Bondi [32] and given in Equation 5, although alternative methods by Sugden and van Krevelen are also commonly employed.[33, 34]

$$\hat{V}_0 = 1.3 \sum_{k=1}^{n} (V_W)_k \tag{5}$$

Here, V_W is the van der Waals volume of various constituent groups on the polymer repeat unit. From Equations 4 and 5 and some experimental observations, we can estimate the

fractional free volume of native polymers; however, this problem quickly becomes more complex when the effects of diluents are considered.

It is useful to consider an estimation of the $\hat{V}$ term in Equation 4, both for cases when experimental observations may be unavailable and for understanding how low molecular weight diluents affect polymer free volume. Some examples are equations proposed by Vrentas[35] or a simplified version later proposed by Ruiz-Treviño and Paul given in Equation 6.[36]

$$\hat{V}_g^m(T) = w_d\hat{V}_l^d(T) + w_p\hat{V}_l^p(T) + \left(\frac{d\hat{V}_l^m}{dT} - \frac{d\hat{V}_g^m}{dT}\right)\left(T_g^m - T\right) \quad (6)$$

Here, $\hat{V}_g^m(T)$ is the specific volume of the glassy mixture at a temperature, T, below the mixture glass transition temperature, T_g^m, w_d is the weight fraction of diluent, $\hat{V}_l^d(T)$ is the specific volume of the pure diluent in the equilibrium liquid state, w_p is the weight fraction of polymer, $\hat{V}_l^p(T)$ is the specific volume of the pure polymer in the equilibrium liquid state, and$\left(\frac{d\hat{V}_l^m}{dT} - \frac{d\hat{V}_g^m}{dT}\right)$ is the difference in the thermal expansion coefficients of the mixture in the equilibrium liquid and glassy states, respectively. An illustration of how Equation 6 is applied to the free volume of an MMCM system is shown in Figure 1. In Figure 1, the orange highlighted area corresponds to regions of the polymer relatively distant from a cage molecule. The free volume in these regions is assumed to be unchanged from that of the neat polymer. The blue highlighted area is the pore volume of the cage molecule. The green highlight area corresponds to polymer regions immediately

surrounding cage molecules. The free volume in these regions will deviate from that of the neat polymer due to non-ideal mixing between the cage and polymer.

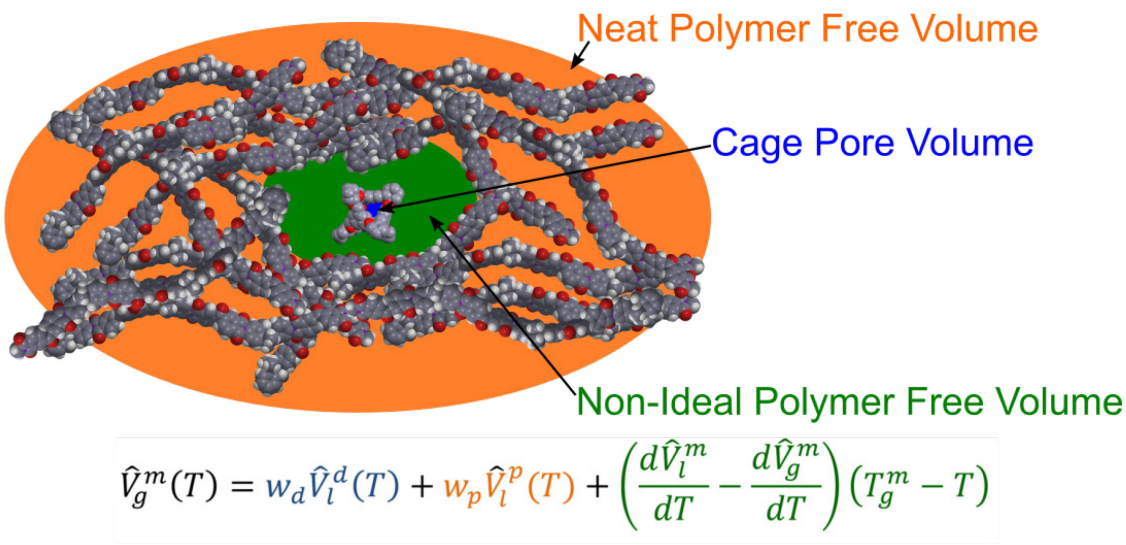

Figure 1: Application of Equation 6 to the three "zones" of free volume in an MMCM system. We note that Equation 6 was originally formulated for describing specific volume but can be considered analogous for our description of free volume. The orange area represents the free volume of the neat polymer, assumed to be unchanged in polymer regions far away from a cage molecule. The blue area is the cage pore volume. The green area is polymer regions immediately surrounding cage molecules, which will be distorted from the neat polymer regions due to non-ideal mixing between the cage and polymer.

When utilizing Equation 6 in cases in which $\hat{V}_l^p(T)$ is not already known, it can be readily estimated from Equations 7, [36] 8, and 9.[34]

$$\hat{V}_l^p(T) = \hat{V}_g^p(T) + \left(\frac{d\hat{V}_g^p}{dT} - \frac{d\hat{V}_l^p}{dT}\right)(T_g^p - T) \tag{7}$$

$$\frac{d\hat{V}_l^p}{dT} = 1 * \frac{10^{-3}\hat{V}_W}{M} \tag{8}$$

$$\frac{d\hat{V}_g^p}{dT} = 0.45 * \frac{10^{-3}\hat{V}_W}{M} \quad (9)$$

186 M is the molecular weight of the polymer repeat unit. Equation 7 can also be applied to
187 diluents, although it was originally in the context of low molecular weight diluents like
188 polymer oligomers. It is unclear whether the concepts of "glassy" or "equilibrium liquid"
189 states can be applied to ASPOC diluents, given their relatively rigid structures. Therefore,
190 we propose Equation 10 for the estimation of the $\hat{V}_l^d$ term in Equation 6.

$$\hat{V}_l^d(T) \cong \hat{V}_{c,s}(T) \cong \hat{V}_c(T) - \hat{V}_{c,p}(T) \quad (10)$$

191 In Equation 10, $\hat{V}_{c,s}(T)$ is specific volume occupied by the cage skeleton at temperature T,
192 $\hat{V}_c(T)$ is the total molecular volume of the cage at T, and $\hat{V}_{c,p}(T)$ is the volume of the
193 internal cage pore (easily determined from diffraction and sorption measurements). $\hat{V}_c$ and
194 $\hat{V}_{c,p}$ are both commonly reported parameters in computational studies of POC structures
195 that should provide a reasonable estimation of the skeletal cage volume, or $\hat{V}_{c,s}$ can be
196 measured directly from density measurements. To complete our calculation of Equation 6,
197 we make the assumption that the thermal expansion of the mixture is approximately equal
198 to that of the polymer so that we arrive at the same approximation used by Ruiz-Treviño
199 and Paul.

$$\left(\frac{d\hat{V}_l^m}{dT} - \frac{d\hat{V}_g^m}{dT}\right) \cong \left(\frac{d\hat{V}_l^p}{dT} - \frac{d\hat{V}_g^p}{dT}\right) \quad (11)$$

200 With the use of Equation 6 to estimate $\hat{V}$ and by taking a weighted average of the
201 $\hat{V}_0$ values for the diluent and polymer, we can nearly estimate the fractional free volume
202 with Equation 4; however, Equation 4 does not consider the effects of diluents with
203 intrinsic porosity. Direct use would underestimate the FFV of ASPOC-filled MMCMs

because the pore volume of the cage is neglected. Hence we propose a slightly modified version of Equation 4 that accounts for the pore volume and the fact that the rigidity of the cage will exhibit some sieving effect on guest molecules.

$$V_{FFV} = \frac{\hat{V} - \hat{V}_0 + w_c \hat{V}_{c,p} \cdot \tanh\left(e \cdot \frac{d_p - d_g}{d_p}\right)}{\hat{V}} \quad (12)$$

Here, d_p is the diameter of the cage window, d_g is the kinetic diameter of the guest, and w_c is the weight fraction of the cage present in the membrane. Although FFV is usually not calculated in the context of the specific guest molecule under investigation, Park and Paul[37] have previously demonstrated how consideration of guest effects can be useful for interpreting permeability data. We believe that it will be particularly important in this context due to potential sieving properties of the cage molecules. Figure 2 illustrates our hypothesis of how free volume should be considered for intrinsically porous molecular fillers. The $\tanh\left(e \cdot \frac{d_p - d_g}{d_p}\right)$ term in the numerator of Equation 12 provides a simple scaling factor to account for the relative sizes of the guest and cage windows. This term of course converges to unity in the limit of no guest and approaches zero as the size of the guest and window approach each other. As the guest size surpasses the window size, the term approaches negative one because the pore volume is now mostly inaccessible to the guest, and the cage is effectively a solid sphere that is occupying otherwise available free volume elements. We note that the proposed functional form was not derived on any theoretical basis but should empirically capture the relationship between the accessible free volume of the cage and guest molecule size. The tanh function was selected instead of a step function because it smoothly passes through zero instead of considering the cage pore volume in a binary manner of accessible or inaccessible. This distinction is likely unimportant for guest

molecules that are either much smaller or much larger than the cage window but should better represent the accessible free volume available to guests that are close in size to the cage window. Guests that are slightly smaller than the pore window are still considered able to access the free volume, but it will be more challenging because the activated process of jumping through the window will become more difficult than for a much smaller guest. Conversely, if guests are slightly larger than the nominal window size, they may still occasionally access the pore interior due to cage flexibility, so it would be incorrect to assume the cage is completely inaccessible.[13, 38, 39]

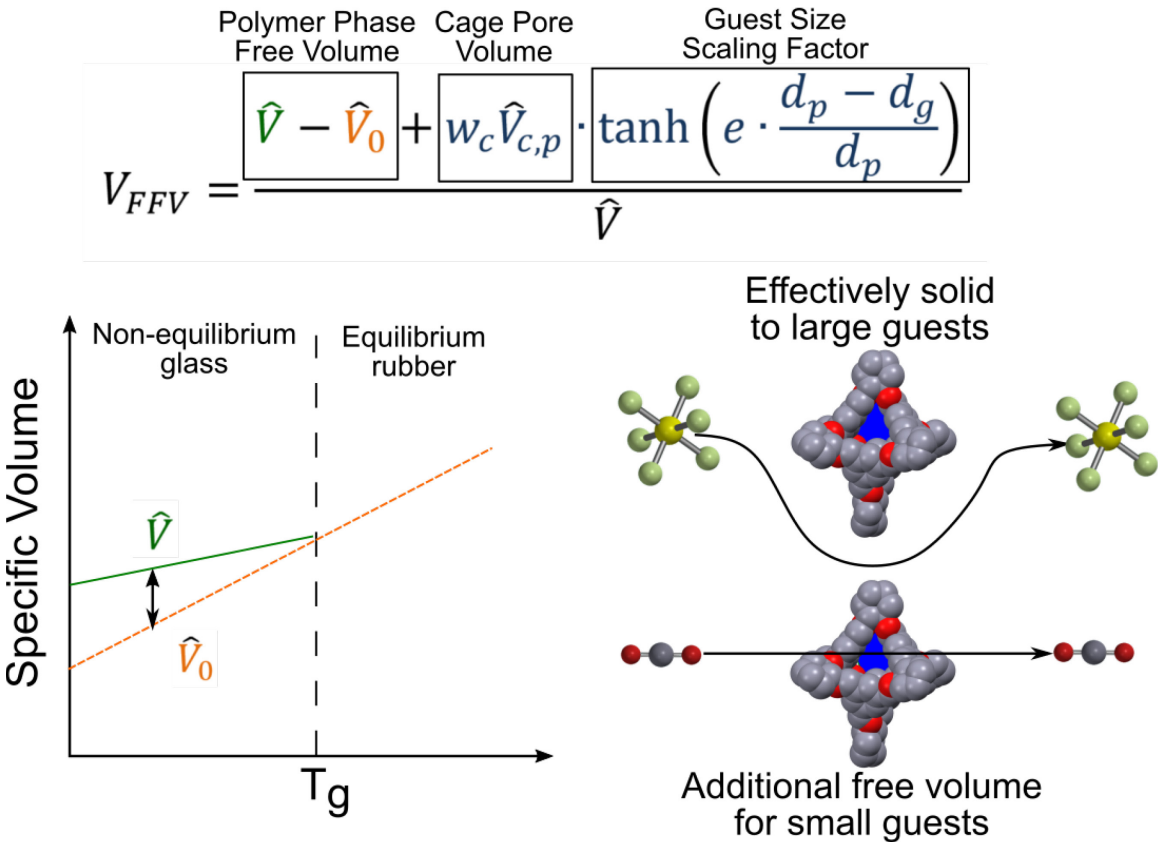

Figure 2: Illustration of the molecular sieving free volume considerations expressed in Equation 12. $\hat{V} - \hat{V}_0$ represents the total free volume of the polymer phase, which is the result of thermal expansion of the polymer from its ideal specific volume at 0 K, as shown in the image in the lower left. The image on the lower right illustrates how the cage will exhibit a sieving effect on guest molecules, so molecular size must be considered to determine in the cage pore volume should be included in free volume calculations or not. The cage will effectively act as a solid impediment to large guests but can be easily accessed by smaller guests.

2.3 Molecular Fillers Effects on Polymer Chain Mobility

While the free volume effect will be important in characterizing the transport effects of molecular fillers, we believe that it alone will be insufficient.[40] The second mechanism

by which ASPOC fillers influence transport is by affecting the mobility of polymer chains. For a permeate to diffuse through a polymer membrane, elements of the chain must have sufficient mobility to allow permeates sufficient space to make a diffusive jump.[30, 41] Antiplasticizers, in addition to their free volume effects, can also lower the energy barriers of secondary relaxations through attractive interactions with the polymer chains.[42-44] This mechanism allows the chains to settle into configurations that are closer to their equilibrium configurations, which of course, raises the energy penalty for shifts to configurations that facilitate penetrant transport. Polymer relaxations are typically referred to as α, β, γ, etc. in order of decreasing temperature. The α relaxation is indicative of large-scale chain movement that is typical of the glass to rubber transition. β relaxations in glassy polymers typically correspond to the relaxation of non-equilibrium packing defects. The γ and lower order relaxations are attributed to motions of single repeat units or various functional groups on repeat units.[45, 46] Clearly, for operation below the glass transition temperature, the nature of the β and lower-order relaxations will be of primary importance. We can measure the onset of these various relaxations with dynamic mechanical analysis

2.4 Net Effect of Molecular Fillers on Transport

Now that we have established the tools with which to study the effects on membrane transport of adding molecular fillers and their effects on free volume and chain mobility, we will hypothesize how these changes affect membrane sorption and diffusivity. We first consider how these hypotheses would affect sorption with the well-known dual-mode adsorption model, shown in Equation 13.

$$\mathbb{S} = k_D p + \frac{C_H' b p}{1 + b p} \tag{13}$$

Here, k_D is the Henry's law constant, p is sorbate pressure (or equivalently concentration), C_H' is the Langmuir capacity constant, and b is the Langmuir affinity constant. The dual-mode model assumes that sorption takes place by two mechanisms, one in which the sorbate is dissolved and governed by Henry's law, and one which occurs in microvoids and is governed by the Langmuir isotherm.[47] Since the Langmuir capacity is the maximum amount of sorbate that can sorb in the microvoids, it should be positively correlated with the free volume.[48] Similarly, we expect the Henry's and affinity terms to be positively correlated with chain mobility, as more mobile chains should be able to better position themselves for favorable sorbate interactions. This is borne out in previous work, where all dual-mode parameters were found to decrease at low antiplasticizer loadings.[49] In our case of using an intrinsically porous antiplasticizer, we expect that the porosity of the filler will counteract this reduction at low loadings to increase net solubility. We note we will not be able to decouple the individual Henry's and Langmuir coefficients of the polymer and filler. We will only be able to observe the overall coefficients of the composite.

We now consider the effects of the ASPOC filler on diffusion. Estimation of the permeability and diffusion coefficient through a polymer membrane is well-established in the literature and usually takes an exponential form, as shown in Equation 14.[29, 50-52]

$$D = A * exp\left(-\frac{B}{FFV}\right) \tag{14}$$

Although Equation 14 provides a useful correlation for many polymer-penetrant combinations, free volume alone has been shown to be insufficient for correlating permeation and diffusion in some cases.[45, 53] In these cases, we believe that the dynamics of chain mobility may not be adequately considered. Koros and co-workers have noted a higher diffusivity of oxygen in PET compared to PEF, even though PEF has a

higher FFV. They attribute this to the higher mobility of the phenyl ring-flipping in PET compared to the furan moiety in PEF.[30] Relating this general concept back to the current work, we predict that diffusion through the polymer phase will be initially retarded at low ASPOC loadings due to increasing chain rigidity, but may increase at higher cage loadings due to net free volume increases.

3. Materials and Methods

3.1 Materials

Matrimid 5218 was purchased from Ribelin. Commercially-available reagents were used as received: 1,3,5-benzenetricarbaldehyde (Manchester Organics); (1R,2R)-1,2-cyclohexanediamine, ethylenediamine, and trifluoroacetic acid (TFA) (Sigma Aldrich).

3.2 CC3 Synthesis

CC3 was prepared as previously reported in its homochiral form.[54] Dichloromethane (100 ml) was layered slowly onto solid triformylbenzene (TFB, 5 g, 30.86 mmol) without stirring at room temperature. Trifluoroacetic acid (1 mL) was added directly to this solution as a catalyst for the imine bond formation. Finally, a solution of (R,R)-1,2-diaminocyclohexane (5 g, 44.64 mmol) in dichloromethane (100 mL) was added to this, again without mixing. The reaction was covered and left to stand. Over 5 days, all of the solid triformylbenzene was used up, and octahedral crystals of CC3 grew on the sides of the glass reaction vessel. The crystalline product was removed by filtration and washed with 95 % ethanol / 5 % dichloromethane.

3.3 ASPOC Synthesis

ASPOC was prepared using a procedure described previously.[10] As-synthesized CC3 (1 g, 0.894 mmol) was dissolved in 100 mL DCM. Ethylenediamine (EDA) (0.269 g, 4.47

mmol) was dissolved into a separate container of 100 mL DCM. A catalytic amount (0.02 g, 2 mole % relative to the number of imine bonds in the original CC3)[55] of TFA was added to the EDA solution as a catalyst. The two solutions were combined into a round bottom flask and stirred at room temperature for seven days. After seven days, the product was isolated by rotary evaporation. The product was immersed in ethyl acetate for three days, replacing with fresh solvent each day, and then dried at 100 °C under a vacuum overnight.

3.4 Scanning Electron Microscopy (SEM)

SEM was performed on a Hitachi SU8010. Cross-sections of membranes were prepared by cryo-fracturing. A small portion of the membrane was soaked in hexane for approximately 15 min then submerged in liquid nitrogen for 5-10 minutes. The membrane portion was broken in two, and the broken edge was placed facing upward on the sample stub. Samples were sputtered with gold using a Quorum Q-150T ES prior to imaging. Images were taken at a working voltage of 5 kV and a current of 10 mA.

3.5 X-ray Diffraction

X-ray diffraction was performed with PANalytical X'Pert PRO Alpha-1 at 40kV and 40 mA with Cu-Kα radiation of 1.54184 Å over a 2θ range of 3° to 50°. Samples were mounted onto a silicon zero background holder. The step size was 0.0041778°, and the scan time was 10.160 s/step.

3.6 Pycnometry

Membrane density was measured via pycnometry and performed by Micromeritics on an AccuPyc II 1340 at room temperature with nitrogen. Fractional free volume was calculated using Eqs. 12 and 5. A weighted average of polymer and cage specific volumes

was used to determine the $\hat{V}_0$ term in Eq. 12. The cage volume was determined from a weighted average of the conformations in the cage mixture based on previous results.[10]

3.7 Thermoelastic Properties

Young's modulus measurement and dynamic mechanical analysis (DMA) were performed on a TA Q800. For both experiments, a strip of membrane approximately 3 cm x 0.3 cm was used. For determining Young's modulus, a static force of 0.001 N and ramp force of 0.1 N/min at 25 °C was used. For DMA, a constant frequency of 1 Hz and temperature ramp method was used with a 0.1% strain over the temperature range -135-400 °C with a 3 °C/min ramp rate. Dynamic scanning calorimetry was performed on a Netzsch STA 449F3 under nitrogen. Samples were cycled from 50-350 °C at 10 °C/min under nitrogen three times. Data from the second ramp to 350 °C was used to determine the glass transition temperature.

3.8 Gas Sorption Measurements

Equilibrium and kinetic gas sorption measurements of carbon dioxide and nitrogen were measured between 0 and ~75 psi in a pressure decay sorption apparatus at 35 °C using approximately 20 mg of membrane samples. A constant testing temperature was obtained by submerging the sample cell in an oil bath. Sample densities measured from helium pycnometry were used in calculations. All gases were assumed to be ideal for the purposes of calculation.

3.9 Gas Permeation Measurements

Permeation of nitrogen, helium, sulfur hexafluoride, and carbon dioxide was measured in a constant volume, variable pressure permeation system at 25, 35, and 45 °C. Permeability was calculated with the slope (after ten lag times) of the permeate pressure

vs. time, $\frac{dp}{dt}$, membrane thickness, ℓ, downstream volume, V, membrane area, A, temperature, T, and transmembrane pressure difference, Δp using Equation 14:

$$\mathbb{P} = \frac{\frac{dp}{dt} \cdot \ell \cdot V}{A \cdot T \cdot \Delta p} \tag{14}$$

An upstream pressure of approximately 75 psi was applied for all measurements.

4. Results and Discussion

4.1 Membrane Morphology

The morphology of the membranes was first investigated to determine if aggregates of cage particles were forming in the membranes. The membranes were visually inspected with SEM as shown in Figure 3. As seen in Figure 3B, the membrane morphology is apparently homogenous up to a magnification of 25,000x at cage loadings of up 5 wt%. Above this loading, globules, presumably of agglomerated cage molecules, are observed in Figure 3C-D. The images suggest that there is a *precipitation point* of the cage within the polymer, above which any additional cage will "crash out" upon membrane vitrification. This observation agrees with previous observations in which the agglomeration of cages at high loadings was hypothesized.[22] In Figure 3C, it appears that there may also be some settling of cage particles during the vitrification process. Based on additional experimental work to be described later in the article, we hypothesize that membranes above the saturation loading form a combined MMCM-MMM morphology in which some ASPOC remains homogeneously dispersed within the polymer phase at the nano-scale but agglomerates from the addition of cage above the saturation loading create a more traditional MMM morphology at the meso-scale (i.e., the cage "precipitates out"). An illustration of this hypothesis is provided in Figure 4. As shown in the figure, when

considering the polymer phase at the nano-scale, the ASPOCs (green) are homogeneously dispersed and maintain a “solid solution” morphology at all loadings, although the amount of cage dispersed throughout the polymer obviously increases. At the meso-scale, the membrane maintains a uniform MMCM morphology at low loadings; however, as the cage loading passes the saturation point within the polymer, agglomerates form throughout the membrane. The result is a more traditional MMM morphology. The MMCM-MMM may or may not exhibit some of the classical interfacial issues commonly associated with MMMs.[56] Based on the images in Figure 3B, it appears that our system leads to a “sieve in a cage” defect around the cage agglomerates, which we expect will lead to a decline in membrane selectivity.

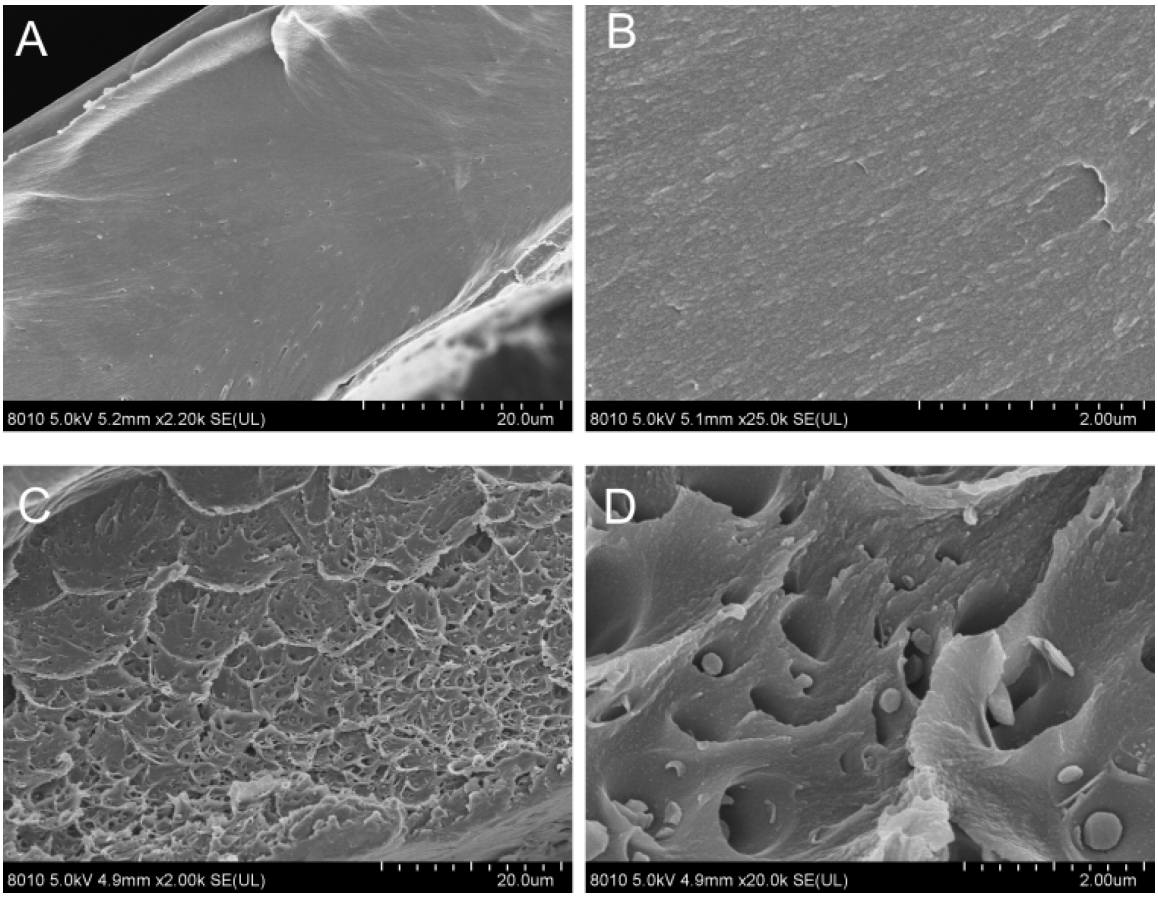

392

393 Figure 3: SEM images of membranes with incorporated ASPOCs. A) and B)
394 Membrane that is 5 wt% ASPOC. C) and D) Membrane that is 10 wt% ASPOC

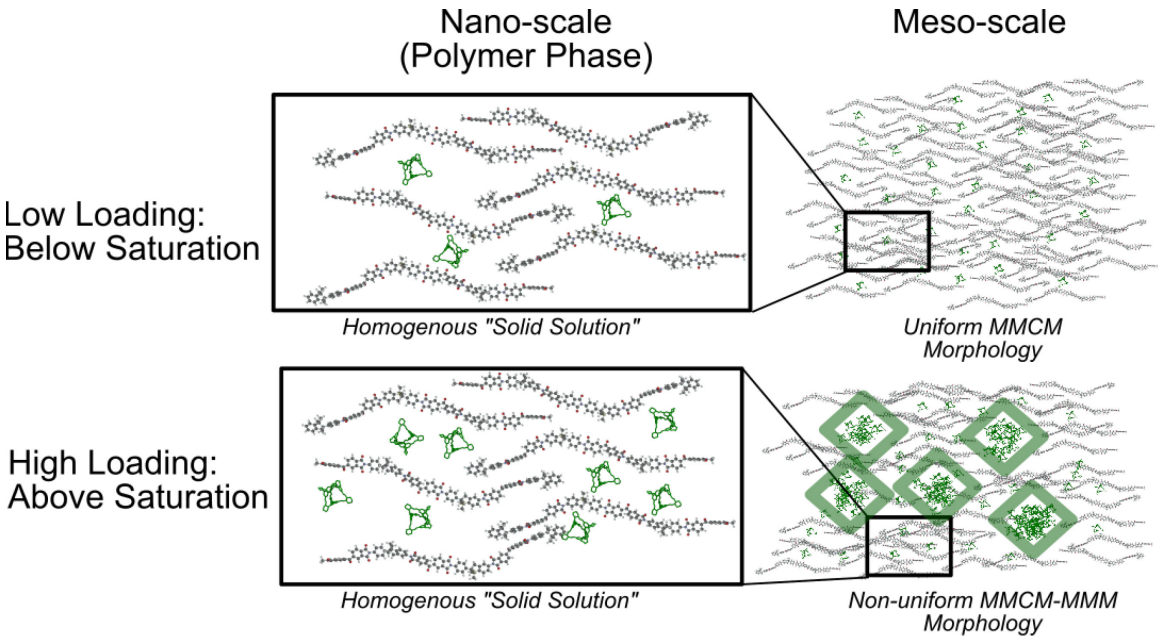

Figure 4: Graphic illustrating the dispersion of ASPOCs in the membrane at different scales and loadings. Polymer chains are in gray and ASPOCs in green. In the upper part of the figure, the MMCM maintains a homogeneous morphology at both the meso- and nano-scales at low loadings. Once the cage "saturation point" is passed in the lower part of the figure, cage agglomerates precipitate out. Cages are hypothesized to remain homogeneously dispersed throughout the polymer phase at the nano-scale (lower left). At the meso-scale, cage aggregates form a combined "MMCM-MMM" morphology. Note that the relative sizes of cages and polymer chains are not to scale.

There is also the possibility that the presence of cages might affect polymer chain packing at higher loadings.[22] This hypothesis was further probed with wide-angle X-ray diffraction, shown in Figure S1. The primary reflection at approximately 15 ° corresponds to an average interchain spacing of ~7.5 Å, relatively close to the spacing measured for similar polyimides.[57] The spacing varies little across the membranes regardless of loading, suggesting that cages do not impact the average interchain spacing. We speculate that this spacing is apparently close enough to the cage molecular diameter (~10 Å)[54] that the cages can sit between chains without increasing their average spacing.

4.2 Membrane Free Volume

Free volume is an important parameter for understanding guest transport in dense membranes. Therefore, we investigated the specific volumes and fractional free volumes of several membranes of varying ASPOC loadings with nitrogen pycnometry. The results are shown in Figure 5. Estimates that assume ideal mixing between the two phases were calculated using Equation 15.

$$\hat{V}_{ideal} = w_c \hat{V}_{c,s} + (1 - w_c)\hat{V}_p \quad (15)$$

Equation 15 represents a weighted average of the experimental, individual specific volumes of the ASPOC and neat Matrimid (and thereby assuming ideal mixing between the two phases) for the specific volume. As seen in Figure 5A, all membranes present a large, positive deviation from ideal mixing behavior. This result is unexpected as previous work with similar, although not the same, POCs has found that they behave like traditional antiplasticizers.[16, 58] The enhanced specific volume effect carries over to the FFV results in Figure 5B. The data reported in Figure 5B were calculated using Equation 12. FFV follows the same trend as specific volume, leading to much higher FFVs than expected. The cages apparently create more free volume within the membrane than expected from a simple weighted average of the neat polymer and cage FFVs. The large discrepancy between the experimental and ideal mixing FFV scenarios also demonstrates how the cages add little additional volume at the low loadings investigated. Instead, their primary mechanism of altering membrane properties seems to be through their effects on the bulk polymer phase.

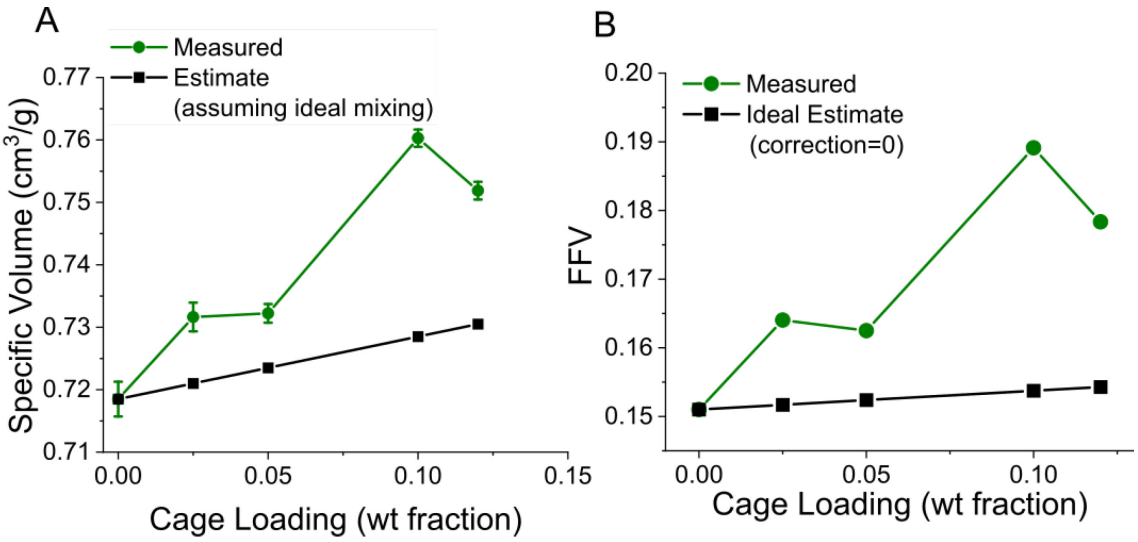

Figure 5: ASPOC-MMCM free volume measurements. A) MMCM specific volume. Experimentally-measured values are indicated with green circles. Estimates using a weighted average of the experimental specific volumes of the ASPOC and neat Matrimid and assuming ideal volume additivity are indicated with black squares. B) Fractional free volume calculated with Equations 5 and 12 using results in A. Green circles represent FFV calculated using the experimentally-measured specific volume and black squares represent estimates that assume ideal mixing and use Equation 15.

4.3 Mechanical/Thermoelastic Properties

The thermoelastic properties of the membrane can provide some insight into its transport behavior. Therefore, we investigate the stress-strain behavior, glass transition temperature, and lower order chain motions with DSC and DMA. The stress-strain behavior and corresponding Young's modulus of several membranes of varying ASPOC loading are shown in Figure S2. In Figure S2, we observe that adding a small amount of ASPOC to the polymer initially makes the membrane less rigid, as evidenced by the more gradual stress-strain response and lower Young's modulus. As the cage loading increases above 2.5 wt%, the membrane apparently becomes more rigid. Although not enough to affect the average interchain spacing, it appears that the addition of a small amount of cage

filler disrupts interactions between polymer chains to make them more mobile. As more cage is added, we hypothesize that attractive interactions between the cage and polymer re-constrict bulk chain mobility to close to original levels.

Increased mobility in the polymer phase is further supported by the measurement of the glass transition temperature (T_g) with dynamic scanning calorimetry, shown in Figure 6. Neat Matrimid exhibits a T_g of 327 °C. Once ASPOC is added, the T_g shifts 6-8 °C downwards for all membranes, indicating that the cages are indeed acting as plasticizers. This result was unexpected since previous work from our lab suggests that POCs typically act as antiplasticizers that restrict chain mobility when incorporated into membranes.[16] Recent computational work has illustrated how variations in cage chemistry can lead to significant differences in membrane properties and performance,[58] so the difference is likely due to the different ASPOC formulation used in this work. This discrepancy underscores the impact of cage chemistry on the final membrane properties. The large-scale increases in chain mobility caused by plasticization are also likely responsible for the "softening" behavior observed in Figure S2. Interestingly, the T_g does not follow the pattern of an initial reduction followed by a gradual increase observed in the Young's modulus, or if it does, it is much more subtle.

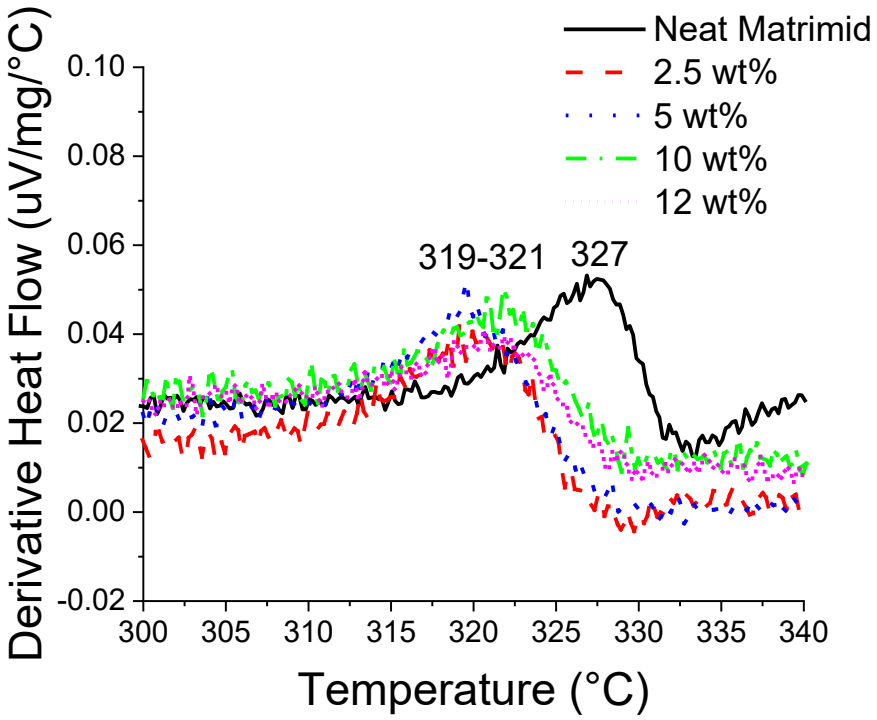

Figure 6: Dynamic scanning calorimetry curves of MMCMs of various weight loadings. Note that the derivative of heat flow with respect to temperture is shown to highlight where the inflection point indicating the glass transition occurs.

We are also interested in chain mobility at smaller scales relevant to the diffusion of guest molecules through the membrane. We probed the mobility of β and γ chain motions with dynamic mechanical analysis at 1 Hz, shown in Figure 7. First, looking at the β motion around 140 °C, we observe that the peak of the neat Matrimid curve occurs at 131 °C. When a small amount of ASPOC is added, the transition shifts upward to 4-19 depending on the cage loading. In the γ transition range, there appears to be a slight decrease in the transition temperature in the MMCMs relative to neat Matrimid, although the experiments are not sensitive enough to be definitive. The increase in the β transition temperature with cage loading is surprising since it displays the opposite trend observed for the T_g. A hypothesis for this contradictory behavior is shown in Figure 8. The top part

of the figure illustrates the neat polymer scenario where chains are highly entangled at the macro-scale, leading to more rigid viscoelastic properties, as observed in Figure S2 and Figure 6. At the nano-scale, chain segments are able to easily relax into free volume elements via the β transition. The bottom part of the figure illustrates our hypothesis when molecular fillers are introduced into the polymer. At the macro-scale, we hypothesize that attractive interactions with the cages partially "untangle" chains relative to the neat polymer. Less entangled chains would presumably have more freedom for the large-scale movements associated with the glass transition, resulting in a lower T_g. We emphasize that the degree of order imposed by the cages is highly exaggerated for clarity in the figure and does not reflect physical reality. At the nano-scale, the molecular fillers block chain movements and prevent relaxation into free volume elements.

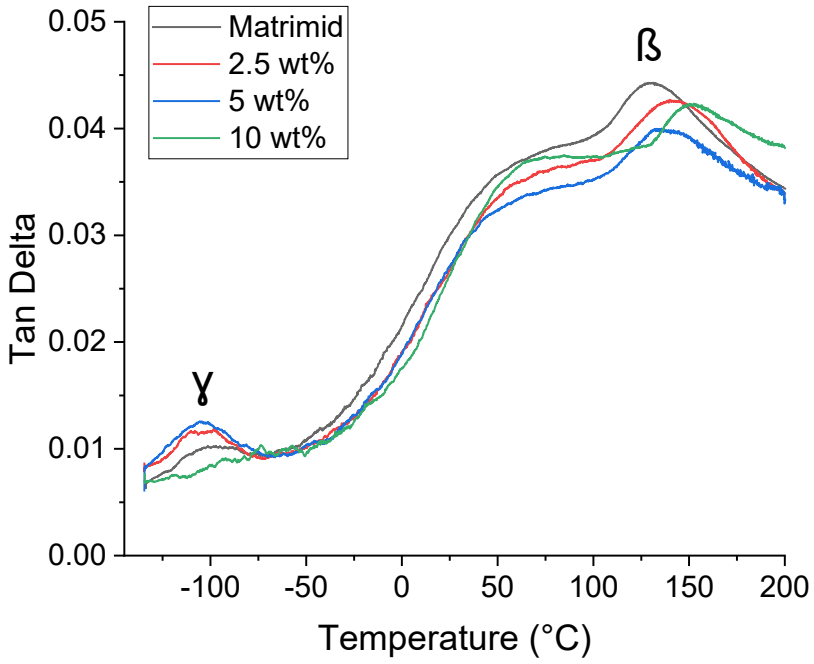

Figure 7: MMCM elastic behavior from DMA at 1 Hz

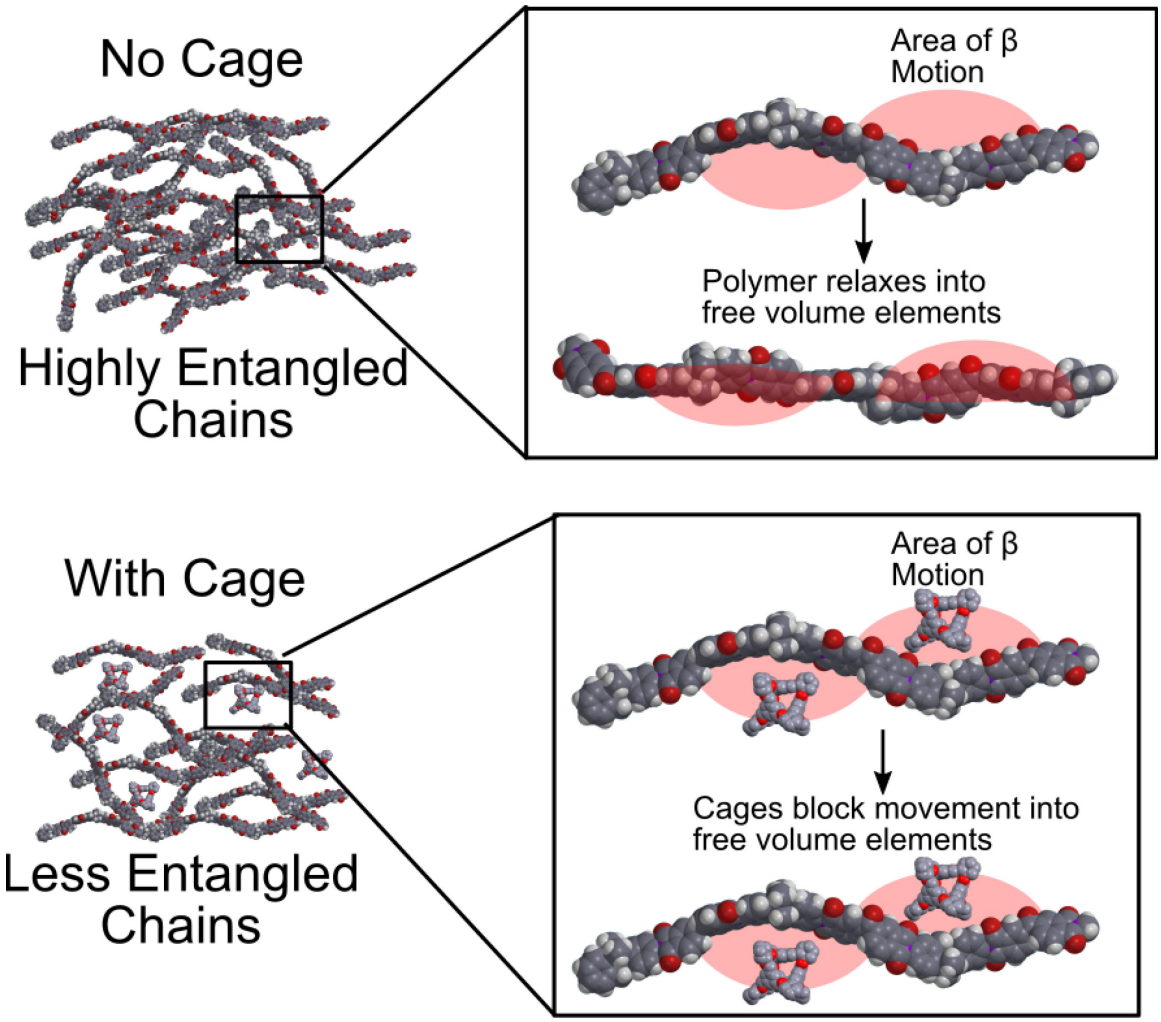

Figure 8: Hypothesis of the effects that molecular fillers have on polymer chain dynamics at varying length scales. (Top) The no cage scenario with highly entangled chains at the macro-scale that can freely relax into free volume elements via β chain motions. (Bottom) Cage presence resulting in less entangled chains at the macro-scale and cages blocking movements into free volume elements at the nano-scale. We emphasize that the "untangling" effect is highly exaggerated in the figure to more effectively illustrate the hypothesis.

4.4 Gas Sorption

As stated earlier, it is important to understand the nature of guest sorption to characterize membrane transport. Isotherms of nitrogen and carbon dioxide at 35 °C are

shown in Figure 9 (top and bottom, respectively). For both gases, we observe that the experimental sorption is far above the weighted average estimate. The excess sorption is likely a result of the enhanced FFV observed earlier, creating more sorption sites. Another interesting aspect is the degree of sorption increase in the MMCMs relative to Matrimid. MMCM N_2 sorption increases by a factor of 5-7. CO_2 only increases by a factor of 2-3, although total sorption remains much higher than N_2. This can partially be explained by guest sorption in the cage sites. The ASPOC exhibits a relatively low CO_2/N_2 sorption selectivity at 5 atm of approximately 2.25, while Matrimid has a much higher selectivity of about 12. Hence, the cages appear to add a significant amount of non-selective sorption capacity to the membrane, both within the cages themselves and by creating additional sorption sites throughout the polymer. In all of these membranes, the ASPOC only comprises a small amount of the total material (< 3 vol%). Even though the cage may be able to adsorb more sorbate per unit mass, the polymer comprises such a large fraction of the membrane that contributions of the ASPOC are negligible in comparison. Therefore, we must focus on how the cage affects the interaction between the sorbate and polymer to understand the implications of the sorption results.

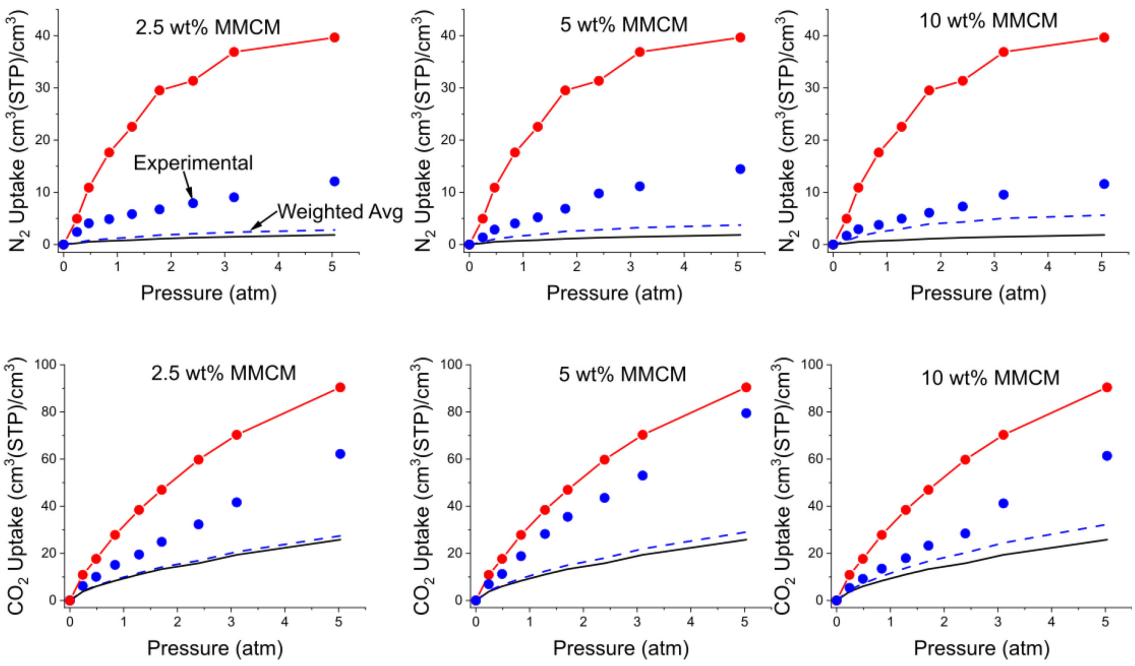

Figure 9: Gas sorption isotherms of nitrogen (top) and carbon dioxide (bottom) from 0 to 5 atm at 35 °C. Points indicate experimental measurements. The blue dotted line denotes the estimated adsorption based on a weighted average of the adsorption of Matrimid (solid black line) and ASPOC (splined red circles).

To gain more insight into the gas-membrane sorption interactions, we fit the isotherms in Figure 9 to Equation 13. The results are presented in Figure 10. For the Henry's constant, we observe a large increase in the case of CO_2. This increase is likely due to the "softening" of the polymer observed in Figure S2 and the lowering of the T_g, resulting in a more rubbery polymer. Sorption in rubbery polymers is well documented to follow Henry-type sorption,[48] so it is sensible that this term would increase relative to the neat polymer. The Langmuir capacity is observed to greatly increase for both N_2 and CO_2, although more for nitrogen relative to the neat polymer value. This result suggests that more micropore sorption sites of lower selectivity are available. The value of C_H' has been shown to be

543 highly correlated to membrane free volume,[59] so the increase for both gases is likely
544 caused by the large increases in FFV seen in Figure 5. The Langmuir interaction parameter
545 of N_2 significantly increases in the MMCMs relative to the neat polymer, likely due to
546 much stronger sorption inside the cages. The Langmuir capacity term of CO_2 does not vary
547 much between the MMCMs and the neat polymer since both Matrimid and the cages
548 exhibit a high affinity for CO_2.

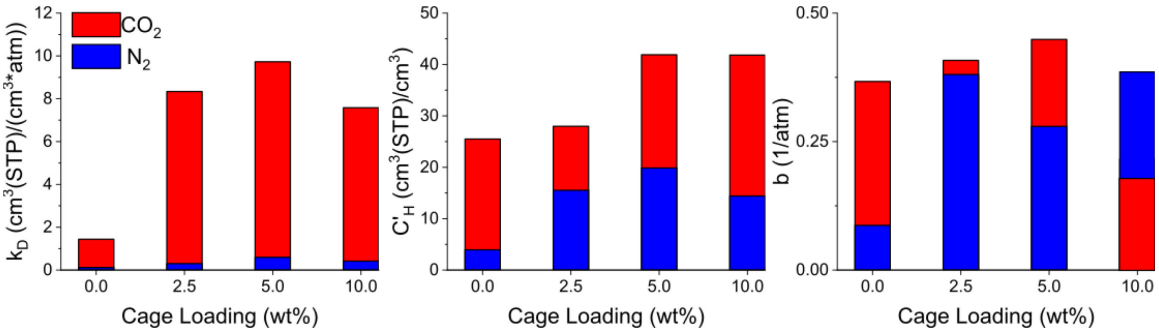

549

550 Figure 10: Dual-mode parameter values for CO_2 and N_2 of MMCMs at various cage
551 loadings.
552

553 *4.5 Gas Permeation*

554 Finally, we investigated the gas transport properties of MMCMs at various weight
555 loadings. Graphs showing the permeability and selectivity of several gas pairs are shown
556 in Figure 11. All measurements in Figure 11 were performed at 35 °C in a constant volume
557 permeation system on pure gases. Permeability error bars were made with three
558 measurements on the same membrane, and propagation of error was used to calculate
559 selectivity error. We also include grayscale cones indicating the range of predictions by the
560 well-known Maxwell model (Equation 16) for mixed matrix membranes.[56]

$$\mathbb{P}_{eff} = P_c \left[\frac{P_f + 2P_c - 2\phi_f(P_c - P_f)}{P_f + 2P_c + \phi_f(P_c - P_f)} \right] \quad (16)$$

Here, $\mathbb{P}_{eff}$ is the effective permeability of the composite, P_c is the permeability of the continuous polymer phase, P_f is the permeability of the filler, and ϕ_f is the volume fraction of the filler. The cones are bounded by lines predicting composite permeability and selectivity assuming the filler has infinite permeability and selectivity (the near-vertical edge) and infinite permeability and selectivity of unity (the horizontal edge). In all three graphs, we can clearly observe that the actual MMCM performance falls far outside the predictions of traditional MMM theory. This result is to be expected because one of the underlying assumptions of the Maxwell model is that both the filler and polymer remain unchanged from their pure component properties. This is not the case, as we have shown with an array of experimental techniques. Thus it is sensible that the Maxwell model would be incapable of predicting MMCM performance.

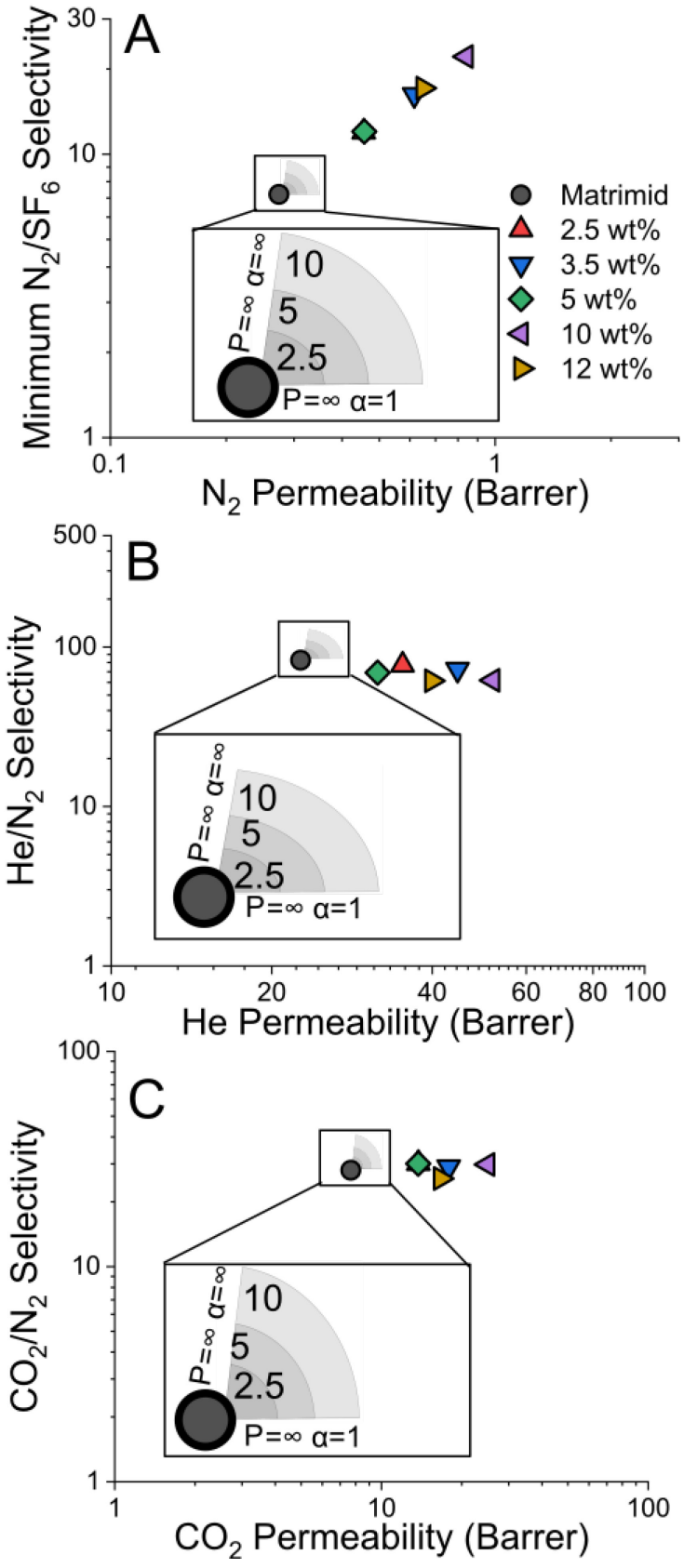
A
Minimum N_2/SF_6 Selectivity
30
10
1
0.1
1
N_2 Permeability (Barrer)
Matrimid
2.5 wt%
3.5 wt%
5 wt%
10 wt%
12 wt%
P=∞ α=∞
10
5
2.5
P=∞ α=1
B
He/N_2 Selectivity
500
100
10
1
10
20
40
60
80
100
He Permeability (Barrer)
C
CO_2/N_2 Selectivity
100
10
1
1
10
100
CO_2 Permeability (Barrer)

572

Figure 11: Gas permeation measurements on MMCMs at various loadings at 35 °C. Measurements were made with pure gases in a constant volume measurement system. Permeability error bars were made with three measurements on the same membrane and propagation of error was used to calculate selectivity error. Error bars are present but are smaller than the points on the graphs. Insets with gray scale cones show the range of predictions from the Maxwell model at the indicated weight loadings (which were converted to volume loadings for calculations). Calculations assuming the filler had infinite permeability and either infinite selectivity (indicated by the near vertical edge of the cones) or a selectivity of unity (indicated by the horizontal edge of the cones) were used to calculate a range of predictions for possible filler selectivities. A) Pure component permeability and selectivity of He over N_2 Note that the point denoting the 2.5 wt% MMCM is obscured by the 5 wt% membrane. B) Pure component permeability and selectivity of N_2 and SF_6. Note that for all membranes, the rate of SF_6 permeation was indistinguishable from the system leak rate and was taken to be 0.038 Barrer as an upper bound. C) Pure component permeability and selectivity of N_2 and CO_2. Note that the point denoting the 2.5 wt% MMCM is obscured by the 5 wt% membrane.

Starting with Figure 11A, we compare the helium permeability and helium/nitrogen selectivity of several MMCMs of increasing cage loading. Although helium permeability varies between membranes, it shows a general increasing trend with cage loading while selectivity steadily decreases. Both helium (kinetic diameter 2.6 Å) and nitrogen (kinetic diameter 3.64 Å) are much smaller than the nominal diameter of the cage window (5-6 Å), so there should be no sieving effect from the cage. They both apparently also benefit from the enhanced free volume and macro-scale chain mobility while not being hindered by the smaller-scale rigidification described previously.

In the case of N_2/SF_6 separation in Figure 11B, we instead observe steady increases in both nitrogen permeability and selectivity. We note that SF_6 permeation was indistinguishable from the leak rate in our system for all membranes. Its permeability was conservatively taken to be equal to the leak rate at 0.038 Barrer. We report only a minimum selectivity based on the upper limit SF_6 permeability. Therefore, the selectivity increase is

605 driven solely by the increases in nitrogen permeability; however, the actual selectivities are
606 almost certainly higher than those we report. SF_6 (kinetic diameter 5.5 Å) is much larger
607 than nitrogen. Although it may be able to enter the cage cavity due to structural flexibility,
608 it is probably mostly rejected from the cages, unlike nitrogen. Additionally, SF_6 likely faces
609 considerable diffusive resistance in the polymer phase due to smaller-scale rigidification
610 that we have observed via DMA measurements. While we cannot report actual selectivities,
611 it is still impressive that ASPOCs can increase nitrogen permeability up to 3x without
612 sacrificing selectivity towards a component that is only 2 Å larger.

613 In Figure 11C, we compare the permeabilities of nitrogen and carbon dioxide.
614 Surprisingly, we observe increases in both CO_2 permeability and CO_2/N_2 selectivity up to
615 10 wt% cage loading. Both N_2 and CO_2 are significantly smaller than the cage pore
616 window, so it is unlikely they experience an appreciable degree of molecular sieving from
617 the cage. Instead, we will examine these results with the assistance of the sorption
618 isotherms in Figure 9. Figure 12 compares the CO_2 and sorption coefficients (left) and
619 diffusivities (right) and their respective selectivities towards nitrogen under the same
620 conditions as the permeation measurements. Diffusion coefficients were calculated by
621 dividing the permeability by the sorption coefficient as in Equation 1. On the left side of
622 Figure 12, we observe the same CO_2 sorption trend as before. CO_2 sorption initially
623 experiences a boost at low cage loadings that becomes less pronounced as the matrix
624 tightens under the influence of restrictive interactions with the cages at higher loadings.
625 The permeability boost in Figure 11C is apparently the result of enhanced sorption capacity
626 in the membrane. Conversely, the sorptive selectivity steadily decreases. It appears that the

cages impart a significant amount of sorption capacity, but this additional capacity is increasingly non-selective.

On the right side of Figure 12, we observe that the CO_2 diffusivity changes little with cage loading; however, the diffusive selectivity dramatically increases from 2 to around 6. Importantly, diffusivity plays such a significant role in overall transport that the increase in diffusive selectivity is enough to offset the decrease in sorption selectivity and result in a net permeation selectivity increase. The enhancement in diffusion selectivity is unexpected considering the results presented earlier that indicate that the polymer is largely less rigid as a result of the cages. The diffusion selectivity enhancement is likely due to the restriction in the β chain motions reducing the transient movements that enable diffusive jumps through the membrane.

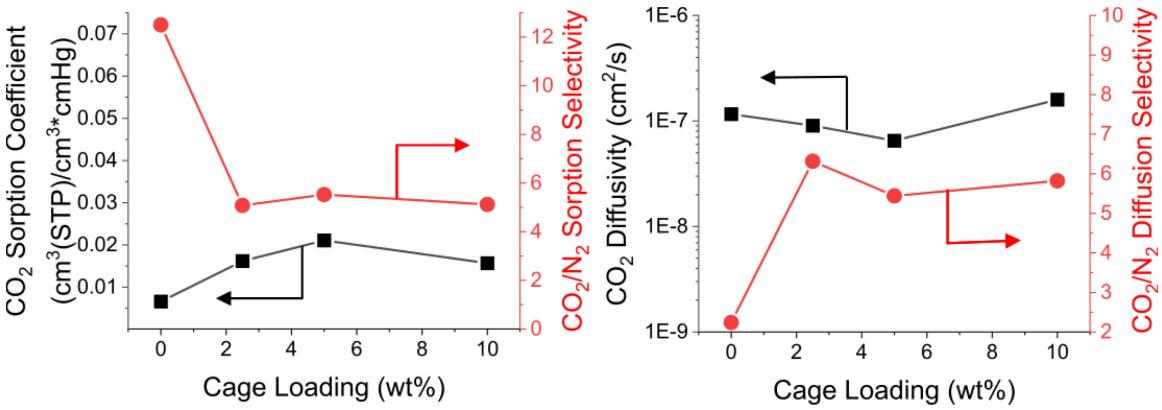

Figure 12: MMCM transport parameters. (Left) Sorption coefficients and sorption selectivities, (Right) diffusivities and diffusion selectivities

Examing the energetics of transport can also provide useful information on how the cages affect permeation properties. Figure S3 shows how the permeation activation energies ($E_{A,\mathbb{P}}$) of nitrogen, helium, and carbon dioxide change with cage loading. Activation energies were calculated from least-squares fitting of Arrhenius plots made

using Equation 2. Gas permeation was measured at 25, 35, and 45 °C. The permeation results used to generate the data in Figure S3 are given in Table S1. The $E_{A,\mathbb{P}}$ of helium varies little with cage loading. This observation indicates that either the changes in sorption and diffusion energetics balance each other out or, more likely, the presence of the cage does not have an appreciable effect on the helium transport energetics. Helium is, in general, such a weakly sorbing species that it is unlikely that the presence of cages would have an appreciable effect on the sorption behavior.[60] Similarly, helium diffusion is already among the least sensitive to polymer motions due to its small size that neither the cages nor their effects on the bulk polymer would not have much effect. The permeation activation energy of CO_2 shows a little more variation than helium, with the $E_{A,\mathbb{P}}$ increasing from 10.6 kJ/mol in neat Matrimid to 15.2 in the 2.5 wt% MMCM. The $E_{A,\mathbb{P}}$ of CO_2 then drops off somewhat and rises again. These small variations are probably the result of the competing effects of enhanced sorption capacity facilitating permeation and increased chain rigidity hindering it or perhaps experimental error. This hypothesis cannot be confirmed without more information on the sorption and diffusion energetics but would be in agreement with the results in Figure 12, where the sorption and diffusion coefficients were observed to be non-monotonic with respect to cage loading. Interestingly, the nitrogen $E_{A,\mathbb{P}}$ declines significantly with cage loading. N_2's greatly increased sorption capacity with cage loading apparently lowers the energy barrier of permeation to a much greater degree than any impediment from chain rigidification raises it, so that the net effect is a lowering of the $E_{A,\mathbb{P}}$.

5. Conclusions

In this work, we have thoroughly characterized the effects of intrinsically porous molecular fillers on membrane physical and transport properties. We found that there is a saturation loading of cages within polymers and that past this loading, excess cages will agglomerate and form an "MMCM-MMM" morphology. We also found that MMCM "solid solutions" are highly non-ideal. Interactions between the filler and polymer lead to positive deviations in specific volume from what would be expected in an ideal mixing scenario. These interactions also significantly affect polymer chain rigidity. Curiously, the cages have the opposite effect depending on the scale of observation. MMCM T_g's were found to be depressed from the neat polymer, indicating plasticization and reduced chain rigidity at the macro-scale, but the onset of the β transition increased, indicating increased chain rigidity at the molecular scale. In the separation of CO_2 and N_2, the presence of cages was found to increase both permeability and selectivity. The permeability enhancement was driven by increased sorption throughout the membrane polymer phase. The selectivity enhancement was found to result from increased diffusion selectivity, likely caused by rigidification of the β motions. The permeation activation energy was observed to vary little with cage loading in the cases of helium and carbon dioxide but decreased significantly for nitrogen.

When porous, molecular fillers are incorporated into polymeric membranes to make MMCMs, several membrane properties change. These properties are often competing with respect to their effects on gas transport, making a fundamental understanding of structure-property relationships difficult. In this work, we attempt to decouple some of these competing effects so that we can further develop our understanding of this exciting new

692 membrane class. Based on the results presented earlier, we propose some guiding
693 principles for future work in this area:

694 1. We often refer to MMCMs as “solid solutions.” Like any solution, there is a
695 saturation loading, in this case, the maximum amount of cage that can be
696 considered to be “dissolved” in the polymer. Any cage added past this threshold
697 will precipitate out and form an “MMCM-MMM” morphology that will be
698 subject to the interfacial issues commonly observed in traditional MMMs. This
699 threshold is relatively low (below 10 wt% for the system studied here) but may
700 be able to be raised with appropriate polymer-filler matching or filler
701 functionalization.
702 2. MMCMs are a completely distinct membrane class from traditional MMMs and
703 should be analyzed as such. Traditional MMM permeation theory (i.e., the
704 Maxwell model) is not appropriate for MMCMs because they violate the
705 assumption that the continuous and filler phases do not interact.
706 3. Molecular fillers significantly alter bulk polymer properties, altering the
707 membrane transport properties. Any attempt to estimate the performance of a
708 polymer/molecular filler matching *a priori*, like with the Maxwell model for
709 MMMs, will likely need to start with molecular simulations to investigate the
710 composite physical properties, namely the free volume and chain mobility.
711 Performance estimates may be able to be made from there based on the
712 performance of the neat polymer.
713 4. Molecular fillers primarily alter transport properties through their effects on the
714 bulk polymer, especially when present at the low loadings investigated here.

Therefore, the relationship between cage external functionality and transport properties should be heavily investigated when optimizing a given polymer/molecular filler matching for a given separation.

5. Like MMMs, MMCMs' separation performance will ultimately be limited by the performance of the neat polymer. They are a method to make a good polymer better but cannot enable a low-performing polymer to compete with the state-of-the-art.

We note some key limitations in our development of these guidelines. These guidelines are based on extensive characterization of only one polymer/filler system. Given the importance of intermolecular interactions between the filler and polymer on the final membrane performance, alterations to these guidelines may be required based on the specific system under investigation. As the field matures and our understanding of the relationship between cage chemistry and membrane performance grows, this point will become more evident. Additionally, gas permeation measurements, while encouraging, were performed on pure gases. Mixed gas performance, especially the sorption and diffusion behavior, will almost certainly vary from the results presented here and may require alteration to our analysis as given. However, we believe that our interpretation of the available data thus far will provide an important foundation for future researchers who choose to study this promising membrane class.

Acknowledgements

The authors thank the National Science Foundation (CAREER) for funding this research. This work was performed in part at the Georgia Tech Institute for Electronics and Nanotechnology, a member of the National Nanotechnology Coordinated Infrastructure (NNCI), which is supported by the National Science Foundation (Grant ECCS-2025462).

Notes

The authors declare no competing financial interest.

REFERENCES

[1] T. Tozawa, J.T. Jones, S.I. Swamy, S. Jiang, D.J. Adams, S. Shakespeare, R. Clowes, D. Bradshaw, T. Hasell, S.Y. Chong, C. Tang, S. Thompson, J. Parker, A. Trewin, J. Bacsa, A.M. Slawin, A. Steiner, A.I. Cooper, Porous organic cages, Nature Materials, 8 (2009) 973-978.

[2] P. Kumar, D.W. Kim, N. Rangnekar, H. Xu, E.O. Fetisov, S. Ghosh, H. Zhang, Q. Xiao, M. Shete, J.I. Siepmann, T. Dumitrica, B. McCool, M. Tsapatsis, K.A. Mkhoyan, One-dimensional intergrowths in two-dimensional zeolite nanosheets and their effect on ultra-selective transport, Nature Materials, 19 (2020) 443-449.

[3] R. Banerjee, A. Phan, B. Wang, C. Knobler, H. Furukawa, M. O'Keeffe, O.M. Yaghi, High-Throughput Synthesis of Zeolitic Imidazolate Frameworks and Application to CO2 Capture, Science, 319 (2008) 939.

[4] R.M. Barrer, V.H. Shanson, Dianin's compound as a zeolitic sorbent, Journal of the Chemical Society, Chemical Communications, (1976) 333-334.

[5] J.L. Atwood, L.J. Barbour, A. Jerga, A New Type of Material for the Recovery of Hydrogen from Gas Mixtures, Angewandte Chemie International Edition, 43 (2004) 2948-2950.

[6] K. Jie, M. Liu, Y. Zhou, M.A. Little, A. Pulido, S.Y. Chong, A. Stephenson, A.R. Hughes, F. Sakakibara, T. Ogoshi, F. Blanc, G.M. Day, F. Huang, A.I. Cooper, Near-Ideal Xylene Selectivity in Adaptive Molecular Pillar[n]arene Crystals, Journal of the American Chemical Society, 140 (2018) 6921-6930.

[7] M.B. Dewal, M.W. Lufaso, A.D. Hughes, S.A. Samuel, P. Pellechia, L.S. Shimizu, Absorption Properties of a Porous Organic Crystalline Apohost Formed by a Self-Assembled Bis-Urea Macrocycle, Chemistry of Materials, 18 (2006) 4855-4864.

[8] M.W. Schneider, H.-J. Siegfried Hauswald, R. Stoll, M. Mastalerz, A shape-persistent exo-functionalized [4 + 6] imine cage compound with a very high specific surface area, Chemical Communications, 48 (2012) 9861-9863.

[9] G. Zhang, O. Presly, F. White, I.M. Oppel, M. Mastalerz, A Permanent Mesoporous Organic Cage with an Exceptionally High Surface Area, Angewandte Chemie International Edition, 53 (2014) 1516-1520.

[10] M.P. Rivera, M. Liu, D. He, R.P. Lively, Tuning Material Properties of Porous Organic Cage CC3 with Postsynthetic Dynamic Covalent Chemistry, European Journal of Organic Chemistry, 2022 (2022) e202101507.

[11] S.Y. Chong, A.I. Cooper, 6.07 - Porous Organic Cages, in: J.L. Atwood (Ed.) Comprehensive Supramolecular Chemistry II, Elsevier, Oxford, 2017, pp. 139-197.

776 [12] L. Chen, P.S. Reiss, S.Y. Chong, D. Holden, K.E. Jelfs, T. Hasell, M.A. Little, A.
777 Kewley, M.E. Briggs, A. Stephenson, K.M. Thomas, J.A. Armstrong, J. Bell, J. Busto, R.
778 Noel, J. Liu, D.M. Strachan, P.K. Thallapally, A.I. Cooper, Separation of rare gases and
779 chiral molecules by selective binding in porous organic cages, Nature Materials, 13 (2014)
780 954.

781 [13] E. Jackson, M. Miklitz, Q. Song, G.A. Tribello, K.E. Jelfs, A Computational
782 Evaluation of the Diffusion Mechanisms for C8 Aromatics in Porous Organic Cages, The
783 Journal of Physical Chemistry C, (2019).

784 [14] G. Zhu, J.-M.Y. Carrillo, A. Sujan, Claudia N. Okonkwo, S. Park, B.G. Sumpter, C.W.
785 Jones, R.P. Lively, Molecular blends of methylated-poly(ethylenimine) and amorphous
786 porous organic cages for SO2 adsorption, Journal of Materials Chemistry A, (2018).

787 [15] Q. Song, S. Jiang, T. Hasell, M. Liu, S. Sun, A.K. Cheetham, E. Sivaniah, A.I. Cooper,
788 Porous Organic Cage Thin Films and Molecular-Sieving Membranes, Advanced Materials,
789 28 (2016) 2629-2637.

790 [16] G. Zhu, F. Zhang, M.P. Rivera, X. Hu, G. Zhang, C.W. Jones, R.P. Lively,
791 Molecularly Mixed Composite Membranes for Advanced Separation Processes,
792 Angewandte Chemie International Edition, 58 (2019) 2638-2643.

793 [17] Z. Zhai, C. Jiang, N. Zhao, W. Dong, P. Li, H. Sun, Q.J. Niu, Polyarylate membrane
794 constructed from porous organic cage for high-performance organic solvent nanofiltration,
795 Journal of Membrane Science, 595 (2020) 117505.

796 [18] A.F. Bushell, P.M. Budd, M.P. Attfield, J.T. Jones, T. Hasell, A.I. Cooper, P.
797 Bernardo, F. Bazzarelli, G. Clarizia, J.C. Jansen, Nanoporous organic polymer/cage
798 composite membranes, Angewandte Chemie International Edition English, 52 (2013)
799 1253-1256.

800 [19] Z. Zhai, N. Zhao, J. Liu, W. Dong, P. Li, H. Sun, Q. Jason Niu, Advanced
801 nanofiltration membrane fabricated on the porous organic cage tailored support for water
802 purification application, Separation and Purification Technology, 230 (2020) 115845.

803 [20] J.D. Evans, D.M. Huang, M.R. Hill, C.J. Sumby, A.W. Thornton, C.J. Doonan,
804 Feasibility of Mixed Matrix Membrane Gas Separations Employing Porous Organic Cages,
805 The Journal of Physical Chemistry C, 118 (2014) 1523-1529.

806 [21] G. Zhu, D. O'Nolan, R.P. Lively, Molecularly Mixed Composite Membranes:
807 Challenges and Opportunities, Chemistry – A European Journal, 26 (2020) 3464-3473.

808 [22] M.P. Rivera, N.C. Bruno, M.G. Finn, R.P. Lively, Organic solvent reverse osmosis
809 using CuAAC-crosslinked molecularly-mixed composite membranes, Journal of
810 Membrane Science, 638 (2021) 119700.

811 [23] T.T. Moore, W.J. Koros, Non-ideal effects in organic–inorganic materials for gas
812 separation membranes, Journal of Molecular Structure, 739 (2005) 87-98.

[24] S. Jiang, L. Chen, M.E. Briggs, T. Hasell, A.I. Cooper, Functional porous composites by blending with solution-processable molecular pores, Chemical Communications (Cambridge), 52 (2016) 6895-6898.

[25] S. Jiang, J.T.A. Jones, T. Hasell, C.E. Blythe, D.J. Adams, A. Trewin, A.I. Cooper, Porous organic molecular solids by dynamic covalent scrambling, Nature Communications, 2 (2011) 207.

[26] J.G. Wijmans, R.W. Baker, The solution-diffusion model: a review, Journal of Membrane Science, 107 (1995) 1-21.

[27] W.J. Jackson Jr., J.R. Caldwell, Antiplasticization. II. Characteristics of antiplasticizers, Journal of Applied Polymer Science, 11 (1967) 211-226.

[28] W.J. Jackson Jr., J.R. Caldwell, Antiplasticization. III. Characteristics and properties of antiplasticizable polymers, Journal of Applied Polymer Science, 11 (1967) 227-244.

[29] Y. Maeda, D.R. Paul, Effect of antiplasticization on gas sorption and transport. III. Free volume interpretation, Journal of Polymer Science Part B: Polymer Physics, 25 (1987) 1005-1016.

[30] S.K. Burgess, J.E. Leisen, B.E. Kraftschik, C.R. Mubarak, R.M. Kriegel, W.J. Koros, Chain Mobility, Thermal, and Mechanical Properties of Poly(ethylene furanoate) Compared to Poly(ethylene terephthalate), Macromolecules, 47 (2014) 1383-1391.

[31] J.S. Lee, W. Madden, W.J. Koros, Antiplasticization and plasticization of Matrimid® asymmetric hollow fiber membranes. Part B. Modeling, Journal of Membrane Science, 350 (2010) 242-251.

[32] A.A. Bondi, Physical properties of molecular crystals liquids, and glasses, (1968).

[33] S. Sugden, CCXXXIV.—Molecular volumes at absolute zero. Part II. Zero volumes and chemical composition, Journal of the Chemical Society (Resumed), (1927) 1786-1798.

[34] D.W. Van Krevelen, K. Te Nijenhuis, Properties of polymers: their correlation with chemical structure; their numerical estimation and prediction from additive group contributions, Elsevier, 2009.

[35] J. Vrentas, J. Duda, H. Ling, Antiplasticization and volumetric behavior in glassy polymers, Macromolecules, 21 (1988) 1470-1475.

[36] F.A. Ruiz-Treviño, D.R. Paul, A quantitative model for the specific volume of polymer–diluent mixtures in the glassy state, Journal of Polymer Science Part B: Polymer Physics, 36 (1998) 1037-1050.

[37] J.Y. Park, D.R. Paul, Correlation and prediction of gas permeability in glassy polymer membrane materials via a modified free volume based group contribution method, Journal of Membrane Science, 125 (1997) 23-39.

[38] T. Mitra, X. Wu, R. Clowes, J.T.A. Jones, K.E. Jelfs, D.J. Adams, A. Trewin, J. Bacsa, A. Steiner, A.I. Cooper, A Soft Porous Organic Cage Crystal with Complex Gas Sorption Behavior, Chemistry – A European Journal, 17 (2011) 10235-10240.

[39] T. Mitra, K.E. Jelfs, M. Schmidtmann, A. Ahmed, S.Y. Chong, D.J. Adams, A.I. Cooper, Molecular shape sorting using molecular organic cages, Nature Chemistry, 5 (2013) 276-281.

[40] S.K. Burgess, O. Karvan, J.R. Johnson, R.M. Kriegel, W.J. Koros, Oxygen sorption and transport in amorphous poly(ethylene furanoate), Polymer, 55 (2014) 4748-4756.

[41] S. Zekriardehani, S.A. Jabarin, D.R. Gidley, M.R. Coleman, Effect of Chain Dynamics, Crystallinity, and Free Volume on the Barrier Properties of Poly(ethylene terephthalate) Biaxially Oriented Films, Macromolecules, 50 (2017) 2845-2855.

[42] L.M. Robeson, J.A. Faucher, Secondary loss transitions in antiplasticized polymers, Journal of Polymer Science Part B: Polymer Letters, 7 (1969) 35-40.

[43] A.S. Maxwell, L. Monnerie, I.M. Ward, Secondary relaxation processes in polyethylene terephthalate–additive blends: 2. Dynamic mechanical and dielectric investigations, Polymer, 39 (1998) 6851-6859.

[44] R.A. Riggleman, J.F. Douglas, J.J. de Pablo, Characterization of the potential energy landscape of an antiplasticized polymer, Physical Review E, 76 (2007) 011504.

[45] S. Singla, H.W. Beckham, M.E. Rezac, Localized chain mobility and gas transport properties of thermoplastic aromatic polymers, Journal of Membrane Science, 208 (2002) 257-267.

[46] A.C. Comer, D.S. Kalika, B.W. Rowe, B.D. Freeman, D.R. Paul, Dynamic relaxation characteristics of Matrimid® polyimide, Polymer, 50 (2009) 891-897.

[47] D.R. Paul, Dual Mode Sorption Model, Encyclopedia of Membranes, (2016) 1-2.

[48] G.K. Fleming, W.J. Koros, Dilation of polymers by sorption of carbon dioxide at elevated pressures. 1. Silicone rubber and unconditioned polycarbonate, Macromolecules, 19 (1986) 2285-2291.

[49] S.K. Burgess, J.S. Lee, C.R. Mubarak, R.M. Kriegel, W.J. Koros, Caffeine antiplasticization of amorphous poly(ethylene terephthalate): Effects on gas transport, thermal, and mechanical properties, Polymer, 65 (2015) 34-44.

[50] M.H. Cohen, D. Turnbull, Molecular Transport in Liquids and Glasses, The Journal of Chemical Physics, 31 (1959) 1164-1169.

[51] J.L. Duda, I. Hadj Romdhane, R.P. Danner, Diffusion in glassy polymers — relaxation and antiplasticization, Journal of Non-Crystalline Solids, 172-174 (1994) 715-720.

[52] J.S. Vrentas, J.L. Duda, H.C. Ling, Free-volume equations for polymer-penetrant diffusion, Journal of Membrane Science, 40 (1989) 101-107.

[53] J.D. Moon, M. Galizia, H. Borjigin, R. Liu, J.S. Riffle, B.D. Freeman, D.R. Paul, Modeling water diffusion in polybenzimidazole membranes using partial immobilization and free volume theory, Polymer, 189 (2020) 122170.

[54] J.T.A. Jones, T. Hasell, X. Wu, J. Bacsa, K.E. Jelfs, M. Schmidtmann, S.Y. Chong, D.J. Adams, A. Trewin, F. Schiffman, F. Cora, B. Slater, A. Steiner, G.M. Day, A.I. Cooper, Modular and predictable assembly of porous organic molecular crystals, Nature, 474 (2011) 367-371.

[55] T.H.G. Schick, F. Rominger, M. Mastalerz, Examination of the Dynamic Covalent Chemistry of [2+3]-Imine Cages, The Journal of Organic Chemistry, 85 (2020) 13757-13771.

[56] R. Mahajan, W.J. Koros, Factors Controlling Successful Formation of Mixed-Matrix Gas Separation Materials, Industrial & Engineering Chemistry Research, 39 (2000) 2692-2696.

[57] C. Bas, C. Tamagna, T. Pascal, N. Dominique Alberola, On the dynamic mechanical behavior of polyimides based on aromatic and alicyclic dianhydrides, Polymer Engineering & Science, 43 (2003) 344-355.

[58] W. Wei, M. Wang, J. Jiang, Molecular Simulation Study on Molecularly Mixed Porous Organic Cage/Polymer Composite Membranes for Water Desalination and Solvent Recovery, ACS Applied Nano Materials, (2021).

[59] W.J. Koros, A.H. Chan, D.R. Paul, Sorption and transport of various gases in polycarbonate, Journal of Membrane Science, 2 (1977) 165-190.

[60] C.A. Scholes, W.X. Tao, G.W. Stevens, S.E. Kentish, Sorption of methane, nitrogen, carbon dioxide, and water in Matrimid 5218, Journal of Applied Polymer Science, 117 (2010) 2284-2289.